Springer

Dear Author,

Here are the proofs of your article.

- You can submit your corrections **online**, via **e-mail** or by **fax**.
- For **online** submission please insert your corrections in the online correction form. Always indicate the line number to which the correction refers.
- You can also insert your corrections in the proof PDF and **email** the annotated PDF.
- For fax submission, please ensure that your corrections are clearly legible. Use a fine black pen and write the correction in the margin, not too close to the edge of the page.
- Remember to note the **journal title**, **article number**, and **your name** when sending your response via e-mail or fax.
- **Check** the metadata sheet to make sure that the header information, especially author names and the corresponding affiliations are correctly shown.
- **Check** the questions that may have arisen during copy editing and insert your answers/ corrections.
- **Check** that the text is complete and that all figures, tables and their legends are included. Also check the accuracy of special characters, equations, and electronic supplementary material if applicable. If necessary refer to the *Edited manuscript*.
- The publication of inaccurate data such as dosages and units can have serious consequences. Please take particular care that all such details are correct.
- Please **do not** make changes that involve only matters of style. We have generally introduced forms that follow the journal's style.
  Substantial changes in content, e.g., new results, corrected values, title and authorship are not allowed without the approval of the responsible editor. In such a case, please contact the Editorial Office and return his/her consent together with the proof.
- If we do not receive your corrections **within 48 hours**, we will send you a reminder.
- Your article will be published **Online First** approximately one week after receipt of your corrected proofs. This is the **official first publication** citable with the DOI. **Further changes are, therefore, not possible.**
- The **printed version** will follow in a forthcoming issue.

Please note

After online publication, subscribers (personal/institutional) to this journal will have access to the complete article via the DOI using the URL: http://dx.doi.org/[DOI].
If you would like to know when your article has been published online, take advantage of our free alert service. For registration and further information go to: http://www.link.springer.com.

Due to the electronic nature of the procedure, the manuscript and the original figures will only be returned to you on special request. When you return your corrections, please inform us if you would like to have these documents returned.

Metadata of the article that will be visualized in OnlineFirst

Please note: Images will appear in color online but will be printed in black and white.

ArticleTitle	Phase Stability for the Pd-Si System: First-Principles, Experiments, and Solution-Based Modeling	
Article Sub-Title		
Article CopyRight	The Minerals, Metals & Materials Society and ASM International (This will be the copyright line in the final PDF)	
Journal Name	Metallurgical and Materials Transactions A	
Corresponding Author	Family Name	**Napolitano**
	Particle	
	Given Name	**Ralph E.**
	Suffix	
	Division	Division of Materials and Engineering
	Organization	Ames Laboratory, DOE
	Address	Ames, USA
	Division	Department of Materials Science and Engineering
	Organization	Iowa State University
	Address	Ames, USA
	Email	ren1@iastate.edu
Author	Family Name	**Zhou**
	Particle	
	Given Name	**S. H.**
	Suffix	
	Division	Division of Materials and Engineering
	Organization	Ames Laboratory, DOE
	Address	Ames, USA
	Email	
Author	Family Name	**Huo**
	Particle	
	Given Name	**Y.**
	Suffix	
	Division	Department of Materials Science and Engineering
	Organization	Iowa State University
	Address	Ames, USA
	Email	
Schedule	Received	24 November 2014
	Revised	
	Accepted	

Abstract The relative stabilities of the compounds in the binary Pd-Si system were assessed using first-principles calculations and experimental methods. Calculations of lattice parameters and enthalpy of formation indicate that Pd_5Si-μ, Pd_9Si_2-α, Pd_3Si-β, Pd_2Si-γ, and $PdSi$-δ are the stable phases at 0 K (–273 °C). X-ray diffraction analyses (XRD) and electron probe microanalysis (EPMA) of the as-solidified and heat-

treated samples support the computational findings, except that the PdSi-δ phase was not observed at low temperature. Considering both experimental data and first-principles results, the compounds Pd_5Si-μ, Pd_9Si_2-α, Pd_3Si-β, and Pd_2Si-γ are treated as stable phases down to 0 K (−273 °C), while the PdSi-δ is treated as being stable over a limited range, exhibiting a lower bound. Using these findings, a comprehensive solution-based thermodynamic model is formulated for the Pd-Si system, permitting phase diagram calculation. The liquid phase is described using a three-species association model and other phases are treated as solid solutions, where a random substitutional model is adopted for Pd-fcc and Si-dia, and a two-sublattice model is employed for Pd_5Si-μ, Pd_9Si_2-α, Pd_3Si-β, Pd_2Si-γ, and PdSi-δ. Model parameters are fitted using available experimental data and first-principles data, and the resulting phase diagram is reported over the full range of compositions.

Footnote Information | Manuscript submitted October 15, 2015

Journal: 11661
Article: 3206

Author Query Form

Springer
the language of science

Please ensure you fill out your response to the queries raised below and return this form along with your corrections

Dear Author

During the process of typesetting your article, the following queries have arisen. Please check your typeset proof carefully against the queries listed below and mark the necessary changes either directly on the proof/online grid or in the 'Author's response' area provided below

Query	Details required	Author's response
Front matter	Please confirm the inserted city name is correct and amend if necessary.	
Front matter	Please provide the manuscript submitted date.	
References	Please provide the complete details for th references [1, 31].	
Title	Please check the edit made in the article title and amend if necessary.	
Figure 8	Please provide the part label caption for figure 8c.	
Lin 186	Please check the edits made in the sentence 'Based on a relatively small set of...' and amend if necessary.	

Phase Stability for the Pd-Si System: First-Principles, Experiments, and Solution-Based Modeling

S.H. ZHOU, Y. HUO, and RALPH E. NAPOLITANO

The relative stabilities of the compounds in the binary Pd-Si system were assessed using first-principles calculations and experimental methods. Calculations of lattice parameters and enthalpy of formation indicate that Pd_5Si-μ, Pd_9Si_2-α, Pd_3Si-β, Pd_2Si-γ, and PdSi-δ are the stable phases at 0 K (–273 °C). X-ray diffraction analyses (XRD) and electron probe microanalysis (EPMA) of the as-solidified and heat-treated samples support the computational findings, except that the PdSi-δ phase was not observed at low temperature. Considering both experimental data and first-principles results, the compounds Pd_5Si-μ, Pd_9Si_2-α, Pd_3Si-β, and Pd_2Si-γ are treated as stable phases down to 0 K (−273 °C), while the PdSi-δ is treated as being stable over a limited range, exhibiting a lower bound. Using these findings, a comprehensive solution-based thermodynamic model is formulated for the Pd-Si system, permitting phase diagram calculation. The liquid phase is described using a three-species association model and other phases are treated as solid solutions, where a random substitutional model is adopted for Pd-fcc and Si-dia, and a two-sublattice model is employed for Pd_5Si-μ, Pd_9Si_2-α, Pd_3Si-β, Pd_2Si-γ, and PdSi-δ. Model parameters are fitted using available experimental data and first-principles data, and the resulting phase diagram is reported over the full range of compositions.

DOI: 10.1007/s11661-015-3206-8
© The Minerals, Metals & Materials Society and ASM International 2015

Author Proof

UNCORRECTED PROOF

I. INTRODUCTION

NON-EQUILIBRIUM effects, such as the formation of metastable crystalline phases, deviation from equilibrium compositions, incorporation of crystal defects, and the presence of non-crystalline ordering as observed in quasicrystalline or glassy phases, can give rise to unusual properties in materials. Certainly, applications of metallic glasses have taken advantage of enhanced mechanical properties associated with non-crystalline structure, and the promise of many related performance benefits calls for the navigation of the far-from-equilibrium energetic and dynamic landscape through controlled materials processing and integrated computational materials engineering (ICME).[1] Detailed thermodynamic models are needed here. As a minimum, reliable solution-based descriptions of Gibbs free energy are required for all phases, compositions, and defect structures that may play a role in the relevant transformation kinetics and the competition between crystalline and non-crystalline phases in glass-forming metallic alloys.[2–4]

Glass formation in metals is not a rare phenomenon, and many non-crystalline alloys have been reported to form during rapid cooling from the melt. The Pd-Si-Cu system is of particular interest, having been shown to exhibit a transition from crystalline solidification to non-crystalline solidification (*i.e.,* glass formation) during directional growth at relatively low rates.[5] Indeed, the "bulk glass forming" composition of $Pd_{77.5}Cu_6Si_{16.5}$ (at. pct)[6,7] has been reported to exhibit glass formation in specimens up to 11 mm in diameter.[8] Many intermediate phases have also been observed, but their relative stabilities have not been quantified or effectively integrated into a comprehensive energetic framework for this alloy system, as is required for an understanding of far-from-equilibrium transformations and metastable phase competition. As a subsystem of the Pd-Cu-Si system, we focus presently on the Pd-Si binary. For this system, we use experiments and first-principles calculations to examine relative phase stabilities and then develop a general solution-based thermodynamic description of the system.

The Pd-Si phase diagram was first modeled by Saunders[9] in 1985 and remodeled by Baxi and Massalski[10] in 1991. The most recent thermodynamic description for the Pd-Si system was offered by Du *et al.*,[11] as summarized by the phase diagram shown in Figure 1, providing reasonable agreement with conventional thermal analysis experiments.[12] In light of recent observations involving crystallization from amorphous solid,[13–18] however, we presently revisit this system to examine a few specific points that call for clarification. The first of these involves the Pd_9Si_2-α phase, which is shown in Du's model to exist only between 1037 K and 1073 K (764 °C and (800 °C). However, experimental observations of Pd_9Si_2-α forming from the glass at low

S.H. ZHOU, Assistant Scientist, is with the Division of Materials and Engineering, Ames Laboratory, DOE, Ames. Y. HUO, Graduate Research Assistant, is with the Department of Materials Science and Engineering, Iowa State University, Ames. RALPH E. NAPOLITANO, Alan and Julie Renken Professor, is with the Division of Materials and Engineering, Ames Laboratory, and also with the Department of Materials Science and Engineering, Iowa State University. Contact e-mails: ren1@iastate.edu; ralphn@iastate.edu

Manuscript submitted October 15, 2015.

Journal : MMTA Dispatch : 28-10-2015 Pages : 15
PIPS No. : 3206 ☐ LE ☐ TYPESET
MS Code : ☐ CP ☐ DISK

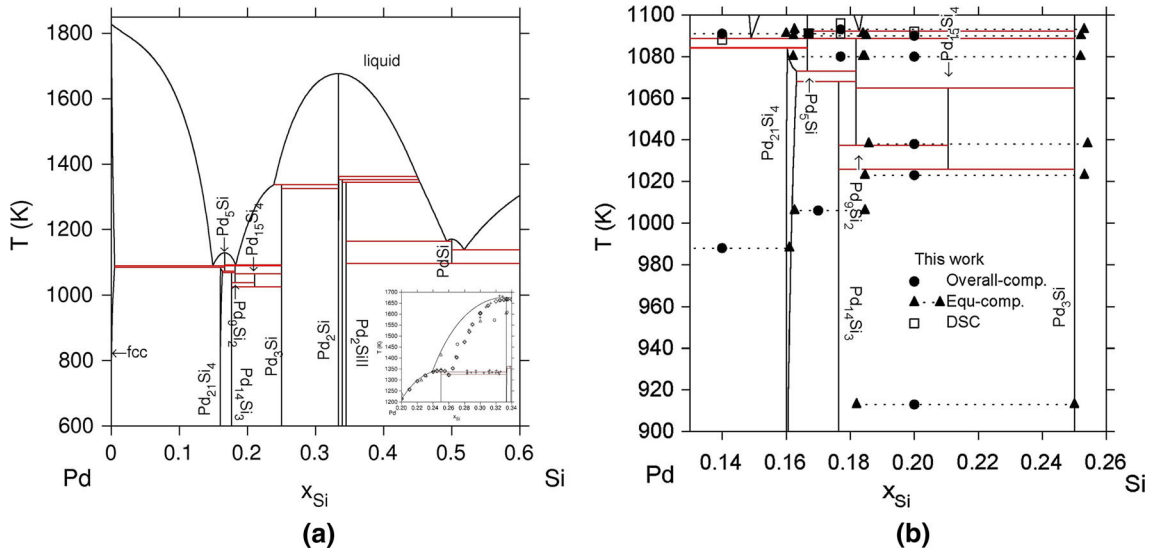

Fig. 1—The Pd-Si binary phase diagram, computed using the parameters by Du *et al.*[11]

temperatures[13–18] suggest that the stability range for this phase might extend to much lower temperatures. The second involves the Pd_3Si-β phase, which is shown by Du's formulation to exhibit peritectic decomposition at 1337 K(1064 °C) in Figure 1, even though a large body of experimental evidence[10,19–23] is available to indicate that this phase melts congruently and that an eutectic point exists at a slightly higher Pd content. The third issue relates to the Pd_2Si-γ phase. Using XRD measurements, Nylund[24] determined that this phase has an Fe_2P prototype (with a corresponding $PdSi_2$ phase exhibiting the same prototype). Massara and Feschotte[12] further investigated the Pd_2Si-γ phase using high temperature XRD measurements and suggested that there are three very similar crystalline structures formed within the composition ranges 33.3 to 34.5 at. pct Si. Accordingly, Du's model[11] includes three phases, centered around the Pd_2Si-γ composition. However, no specific crystal structures have been reported to substantiate the assertion that there are three distinct phases here. Rather, inconsistencies between reports of formation enthalpy (see Figure 2) highlight the need to revisit the available models.[9–11,25–27] In the work reported here, we address each of these three issues and provide other specific points of reference with regard to phase stability in the Pd-Si system. More generally, by incorporating both first-principles calculations and experimental results into our semi-empirical approach, we bring further clarity to the overall thermodynamic description of this system.

II. FIRST-PRINCIPLES CALCULATIONS

To quantify the relative stabilities of the various intermetallic compounds in the Pd-Si system, we compute the zero-Kelvin enthalpies of formation relative to the pure component reference states with a first-principles approach. The total energy E^{θ} is computed for each phase using the Vienna ab initio simulation package (VASP) code[28] employing projector augmented wave method[29] and the high precision generalized gradient approximation (GGA).[30] High precision was used to ensure that the computed absolute energies were converged to a few meV. Spin polarization was enabled. The energy cut-off values, the Monkhorst–Pack k-point mesh size, and the relaxation scheme used for each compound are listed in Table I. The molar enthalpy of formation for a given compound (Pd_aSi_b) is calculated as the difference between the molar energy (E_0^{θ}) of the compound and the linear combination of the pure element reference state molar energies (E_{Pd}^{fcc} and E_{Si}^{dia}), where

$$\Delta H_f^{\theta} = E^{\theta}_{Pd_aSi_b} - [(a(E_{Pd}^{fcc}) + b(E_{Si}^{dia}))/(a+b)]. \quad [1]$$

The calculations were performed for the Pd_5Si-μ, Pd_9Si_2-α, Pd_3Si-β, Pd_2Si-γ, and PdSi-δ phases, as summarized in Table I and plotted in Figure 2. Due to a lack of structural information, energies were not computed for the compounds, $Pd_{21}Si_4$-σ, $Pd_{14}Si_3$, and $Pd_{15}Si_4$. The calculated values of ΔH_f^{β} and ΔH_f^{γ} show good agreement with the measurements of Meschel and Kleppa ($\Delta H_f^{\beta} = -57.9$kJ/mol and $\Delta H_f^{\gamma} = -64.2$kJ/mol).[25] In addition, Figure 2 reveals that the phases Pd-fcc, Pd_5Si-μ, Pd_9Si_2-α, Pd_3Si-β, Pd_2Si-γ, PdSi-δ, and Si-dia are stable, though only marginally, at zero Kelvin. Of note here is the 0 K (−273 °C) stability of Pd_5Si-μ, Pd_9Si_2-α, and PdSi-δ indicated by our calculations. Because each of these phases were reported by Du *et al.*[11] to be stable only over a small range of high temperatures, they deserve additional consideration with respect to their free energy. In the next section, we detail several experiments aimed at assessing the relative stabilities of these phases.

Author Proof
UNCORRECTED

Journal : MMTA Dispatch : 28-10-2015 Pages : 15
PIPS No. : 3206 LE TYPESET
MS Code : CP DISK

Table I. Summary of Results from First-Principles Calculations

Phase-θ	Prototype	Space Group (No.)	ENCUT (eV)	K-Points	ISIF*	ΔH (kJ/mol)
Pd-dia	*C*	Fd-3mO2(227)	313.7	8 8 8	7	109.6
Pd_5Pd-μ	Pd_5Si	$P12_11(4)$	313.7	10 12 14	7	48.7
Pd_5Si-μ			313.7		3	−40.5
Si_5Pd-μ			313.7		7	43.2
Si_5Si-μ			306.7		7	66.4
Pd_9Pd_2-α	Pd_9Si_2	*Pnma*(62)	313.7	8 10 6	7	24.5
Pd_9Si_2-α			313.7		3	−42.7
Si_9Pd_2-α			313.7		7	36.6
Si_9Si_2-α			306.8		7	62.4
Pd_3Pd-β	$F3_3C$	*Pnma*(62)	313.7	9 7 11	7	44.5
Pd_3Si-β			313.7		3	−57.4 (−57.9[25])
Si_3Pd-β			313.7		7	10.6
Si_3Si-β			306.8		7	1.88
Pd_2Pd-γ	Fe_2P	P-62m(189)	313.7	8 8 14	7	186.7
Pd_2Si-γ			313.7		3	−65.1 (−64.2[25])
Si_2Pd-γ			313.7		7	169.4
Si_2Si-γ			306.8		7	148.1
PdPd-δ	*MnP*	*Pnma*(62)	313.7	12 14 10	7	34.7
PdSi-δ			313.7		3	−50.18
SiPd-δ			313.7		7	43.17
SiSi-δ			306.8		7	66.39

Phase-θ	First-principles			Experiment		
	Lattice a b c in Å			Lattice a b c in Å		
Pd-dia	5.8129	5.8129	5.8129	—	—	—
Pd_5Pd-μ	8.8909	8.0184	5.3397	—	—	—
Pd_5Si-μ	8.5757	7.7342	5.1504	8.465[21]	7.485	5.555
Si_5Pd-μ	8.8541	7.9852	5.3176	—	—	—
Si_5Si-μ	8.7127	7.8577	5.2326	—	—	—
Pd_9Pd_2-α	9.4354	7.7461	9.7951	—	—	—
Pd_9Si_2-α	9.1841	7.5398	9.5342	9.0548[21]	7.4188	9.414
Si_9Pd_2-α	9.3946	7.7126	9.7527	—	—	—
Si_9Si_2-α	9.2708	7.6111	9.6242	—	—	—
Pd_9Pd-β	6.0920	8.0253	5.5874	—	—	—
Pd_3Si-β	5.85176	7.6356	5.3544	5.735[41]	7.555	5.26
Si_3Pd-β	5.9783	7.8755	5.4831	—	—	—
Si_3Si-β	5.8130	7.6577	5.3315	—	—	—
Pd_2Pd-γ	8.3439	8.3439	4.4097	—	—	—
Pd_2Si-γ	6.5707	6.5707	3.5523	6.497[24]	6.497	3.432
Si_2Pd-γ	8.6314	8.6314	4.5617	—	—	—
Si_2Si-γ	7.9587	7.9587	4.2061	—	—	—
PdPd-δ	5.9225	3.609	6.4927	—	—	—
PdSi-δ	5.6173	3.386	6.1494	5.6173[42]	3.3909	6.1534
SiPd-δ	5.3175	7.9852	8.8540	—	—	—
SiSi-δ	5.2326	7.8577	8.7127	—	—	—

*3: fully relaxed; 7: cell volume relaxed only.

III. EXPERIMENTS

Test specimens of selected alloy compositions were prepared from the pure elements (0.9999 Pd and 0.99999 Si, by weight) by arc melting and direct-chill freezing on a copper hearth in an argon atmosphere.[31] Each alloy specimen (~15 grams) was arc melted 5 additional times under argon to ensure homogeneity. The as-cast and heat-treated (long-duration) specimens were analyzed using SEM, EPMA/WDS, XRD, and differential scanning calorimetry (DSC). The results, summarized in Tables II and III, show that, in addition to the two terminal solid solutions, four intermetallic phases exhibit ranges of stability as shown in Figures 3, 4, 5, 6, 7, 8, 9, and 10. These results are further summarized in Figure 1, where the test alloy compositions and phase compositions are superimposed on the phase diagram proposed by Du *et al.*[11] Observations and interpretations are discussed below.

Considering first the stability range for the Pd_5Si-μ phase, we examine test specimens with compositions on either side of the expected range, equilibrated at selected

Author Proof
UNCORRECTED PROOF

Journal : MMTA Dispatch : 28-10-2015 Pages : 15
PIPS No. : 3206 LE TYPESET
MS Code : CP DISK

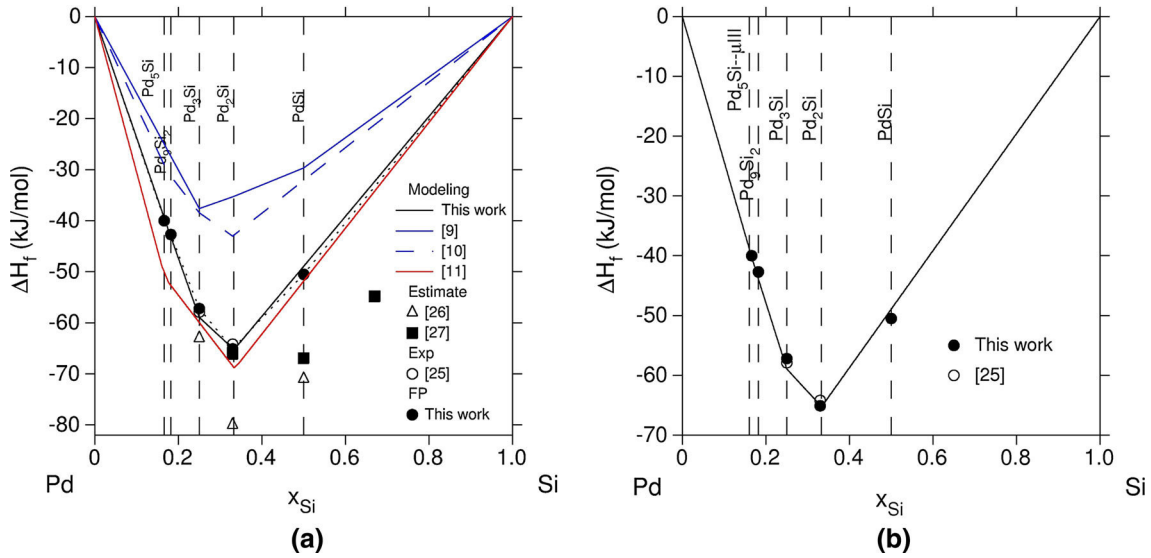

Figure 2—Enthalpy of formation at 298 K (25 °C) calculated using the parameters in Tables V and VI in which Pd_5Si-μ is described with (*a*) $(Pd, Si)_{0.833}(Pd, Si)_{0.167}$ and (*b*) $(Pd, Si)_{0.84}$ $(Pd, Si)_{0.16}$, respectively.

Table II. EPMA Measured Phase Compositions (See Figures 3, 4, 5, 6, 7, 8, 9, and 10)

Comp. at. pct S	ID	Figures	Treatment K (°C)-h	Pd-fcc	Pd_5Si	Pd_9Si_2	Pd_3Si	Pd_2Si	Si-dia
				At. Percent Si/ϖ					
14	H1	3	988 (715)-93	0.7/0.01	15.9/0.42				
	H2	3	1091 (818)-168	1.5/0.08	16.0 /0.10				
16	M1	4(a)	as solidified	not measured	16.4/0.49				
16.7	M2	4(c)	as solidified		16.0/0.06	18.2/0.05			
	H3	5	1091 (818)-168		16.0/0.10	18.3 /0.11			
17	H4	6	1006 (733)-162		16.3/0.13	18.5/0.11			
17.7	M3	—	as solidified		16.7/0	18.9/0.19			
	H5	6	1080 (807)-148		16.2/0.00	18.4/0.00			
	H6	7	1093 (820)-168		16.3/0.09		25.3/0.10		
20	H7	9	913 (640)-210			18.2/0.05	24.8/0.09		
	H8	9(b)	1023 (750)-593			18.5/0.23	25.3/0.27		
	H9	9(b)	1038 (765)-192			18.6/0.11	25.4/0.11		
	H10	9(a)	1080 (807)-148			18.5/0.14	25.2/0.09		
	H11	8	1090 (817)-168		16.2/0	18.5/0.08	25.2/0.15		
64	H12	10	934 (661)-212					32.5/0.65	99.9/0
31	H13	10	1093 (820)-168				25.06/0.10	33.3/0.12	

Standard deviation $\varpi = \sqrt{\frac{(x_1-\bar{x})^2+(x_2-\bar{x})^2+\ldots+(x_n-\bar{x})^2}{n}}$, $\bar{x} = \frac{(x_1+x_2+\cdots+x_n)}{n}$.

Table III. Reaction Onset Temperatures, Measured with DSC on Heating at 40.0 K/min

Overall (At. Percent Si)	Label	Liquidus (K (°C))	Reaction *T* (K (°C))
14	D1	—	1088 (815)
16.7	D2	—	1091 (818)
17.7	D3	1096 (823)	1091 (818)
20	D4	1223 (950)	1092 (819)

temperatures from 988 K to 1093 K (715 °C to 820 °C). As listed in Table II, specimens of 14 at. pct Si (H_1, H_2) yield a fcc/Pd_5Si-μ two-phase equilibrium (see Figure 3) with Pd_5Si-μ compositions of 15.9 to 16.0 at. pct Si. The Pd_5Si-μ was observed in the arc melting 16.0 and 16.7 at. pct Si alloys (M1, M2) (see Figure 4). Specimens of higher Si content in the range of 16.7 to 17.7 at. pct Si (H_3-H_5) yield a Pd_5SiSi-μ/Pd_9Si_2-α two-phase equilibrium (see Figures 5, 6), with Pd_5Si-μ phase compositions of 16.0 to 16.3 at. pct Si. These results indicate a narrow

Author Proof
UNCORRECTED

Journal : MMTA Dispatch : 28-10-2015 Pages : 15
PIPS No. : 3206 LE TYPESET
MS Code : CP DISK

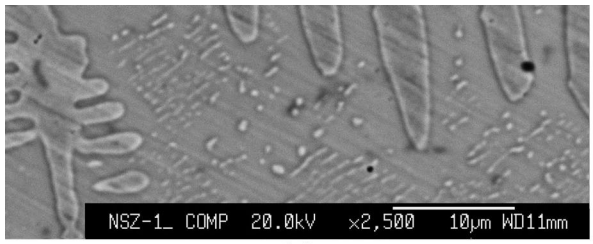

(a)

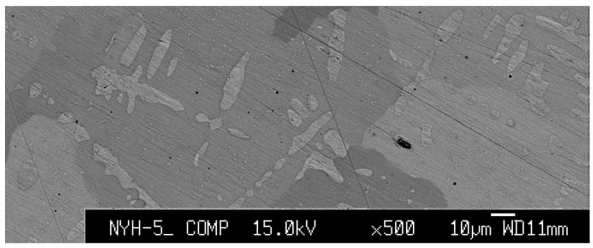

(b)

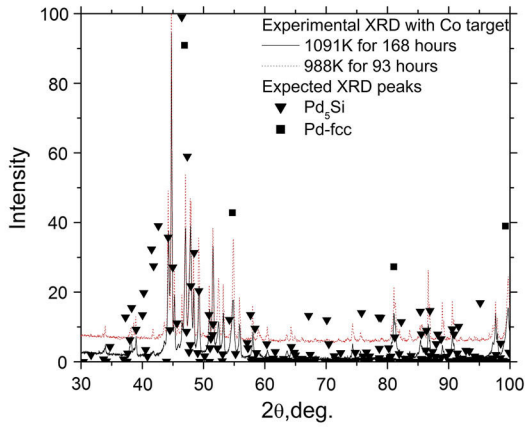

(c)

Fig. 3—EPMA image showing observed microstructure for the Pd-14 at. pct Si alloy treated at (*a*) 988 K (715 °C) for 93 h (H1) and (*b*) 1091 K (818 °C) for 168 h (H2), A: fcc B: Pd_5Si-μ and (*c*) the associated XRD data.

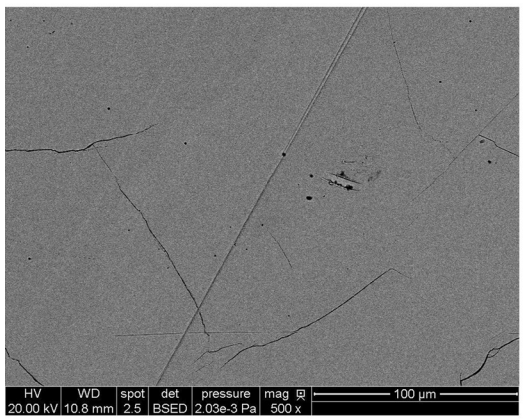

(a)

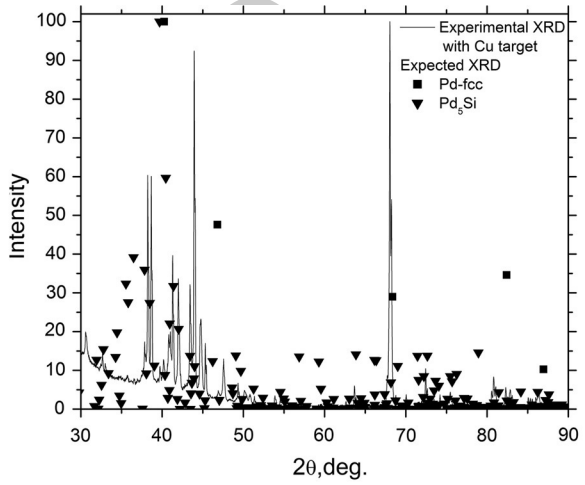

(b)

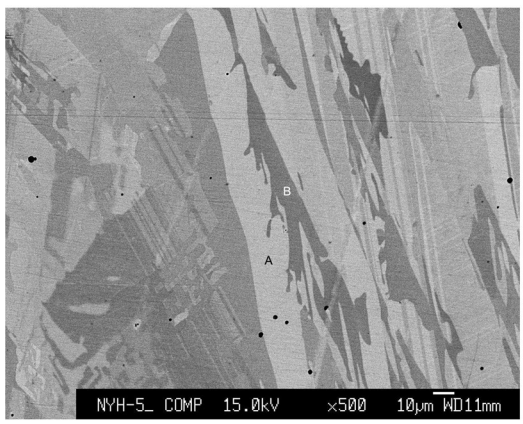

(c)

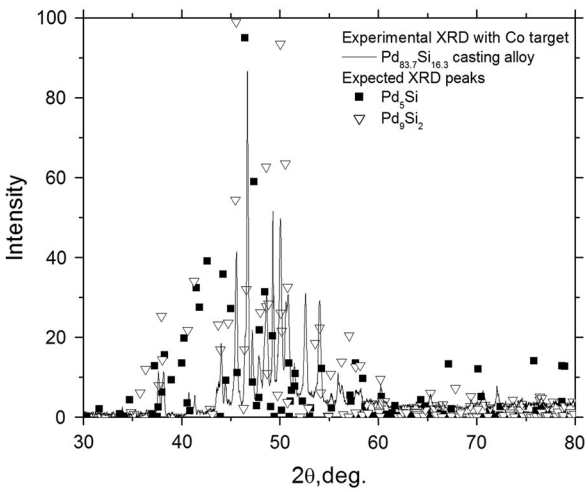

(d)

Fig. 4—(*a*) EPMA image showing observed microstructure and (*b*) the XRD data for the as-cast Pd-16 at. pct Si alloy (M1) and (*c*) EPMA image showing observed microstructure (A: Pd_5Si-μ and B: Pd_9Si_2-α) and (*d*) the XRD data for the Pd-16.7 at. pct Si alloy (M2).

Journal : MMTA Dispatch : 28-10-2015 Pages : 15
PIPS No. : 3206 ☐ LE ☐ TYPESET
MS Code : ☐ CP ☐ DISK

Author Proof

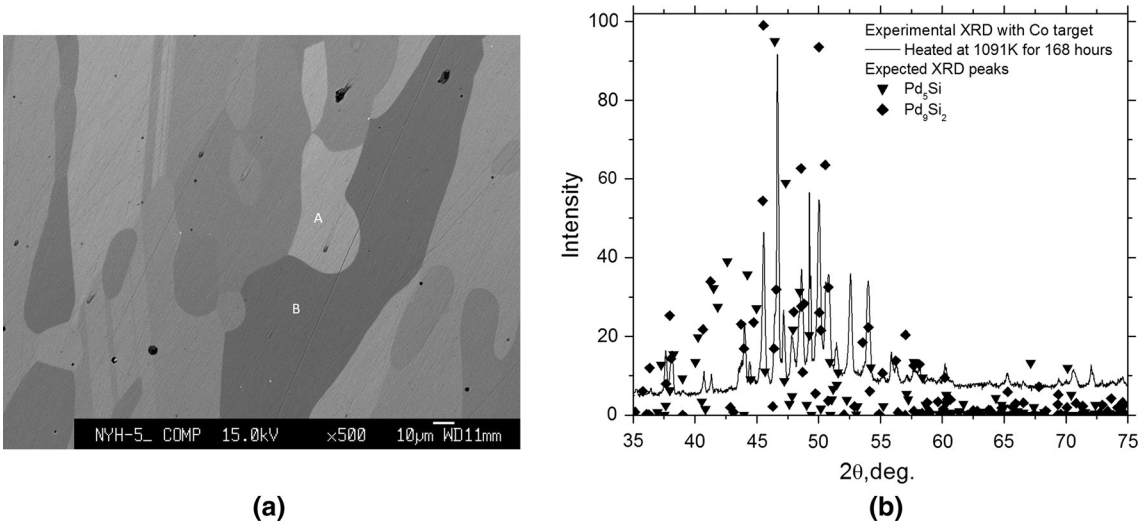

Fig. 5—(*a*) EPMA image showing observed microstructure (A: Pd_5Si-μ and B: Pd_9Si_2-α) and (*b*) XRD data for the Pd-16.7 at. pct Si alloy heat treated at 1091 K (818 °C) for 168 h (H3).

Author Proof

but finite range of solubility for the Pd_5Si-μ phase. Based on a relatively small set of data, we note that this entire range is well below the expected value of 16.7 at. pct, indicated by the stoichiometry of the Pd_5Si-μ phase. Noting that the composition range observed here is consistent with the previously reported $Pd_{21}Si_4$-σ phase[12] for which no structure was determined, we assert here that all of these observations are associated with the same Pd_5Si-μ phase, with stability extending down to 0 K (−273 °C), where a composition of 0.167 is expected. These observations, which we employ in our model, differ substantially from prior reports,[12,23] stating that the Pd_5Si-μ decomposes through eutectoid reaction either to Pd-fcc plus Pd_3Si-β at 1001 K (728 °C)[23] or to $Pd_{21}Si_4$-σ plus Pd_9Si_2-α at 1081 K (808 °C).[12] We note further that the prior report[23] was based on differential thermal analysis employing dynamic heating while our experiments employ long-duration isothermal heat treatments, more likely to approach the equilibrium state.

In a similar manner, the stability of the Pd_9Si_2-α phase was examined using specimen compositions that bracket the stoichiometric value of 18.2 at. pct Si, as listed in Table II. This phase was observed in the solidification structures arising from arc-melting specimens for compositions of 16.7 and 17.7 at. pct Si (M2, M3). The long-duration heat treatment experiments (H3 to H11 in Table II) show the Pd_9Si_2-α phase with an average composition of 18.42 (±0.11) and an upper temperature limit of approximately 1091 K (818 °C). Heat treatments H7 and H8 show that this phase persists as a stable phase down to 913 K (640 °C). Coupled with first-principles calculations which shown that Pd_9Si_2-α is stable to 0 K (−273 °C), we take this phase as stable from 0 K to 1091 K (−273 °C to 818 °C). This is consistent with reported observations of Pd_9Si_2-α crystallization at low temperature from non-crystalline material produced by melt spinning.[13–18]

In reports,[11,12] the $Pd_{14}Si_3$ phase was deemed to be stable from 0 K (−273 °C) up to a pertectoid reaction at 1068 K (795 °C) ($Pd_{21}Si_4$-σ + Pd_9Si_2-α → $Pd_{14}Si_3$). Our results, however, clearly show Pd_5Si-μ/Pd_9Si_2-α equilibrium (with no $Pd_{14}Si_3$) for an overall composition of 17 at. pct Pd at 1006 K (733 °C) (H4 in Table II). The corresponding two-phase microstructure and X-ray data are shown in Figure 6. In addition, DSC results (D2 and D3 in Table III) for compositions of 16.7 and 17.7 at. pct Si show no indication of any reaction until high temperature decomposition reactions involving the Pd_5Si-μ, Pd_9Si_2-α, Pd_3Si-β, and liquid phases. Given that there is no proposed structure for the $Pd_{14}Si_3$ phase, no first-principles calculations were performed. With no compelling evidence to suggest that this phase is stable under any conditions, we do not consider it further in this work, noting that absence as a stable phase certainly does not preclude its observation as a metastable phase in practice.

The $Pd_{15}Si_4$ phase was reported to be stable between 1026 K and 1065 K (753 °C and 792 °C).[11,12] To confirm the stability of the $Pd_{15}Si_4$ phase, the Pd-20.0 at. pct Si alloy was treated at 1038 K (765 °C) for 148 hours (H9) revealing the two phases Pd_9Si_2-σ and Pd_3Si-β microstructure as shown in Figure 9 and in Table II. We conclude that the $Pd_{15}Si_4$ phase reported by Massara and Feschotte[12] is not stable and is not considered further in this work.

As mentioned in Section II, the first-principles results in Figure 2 show that the PdSi-δ phase is a stable phase at low temperature while the experimental investigations[12,20,22] conclude that the PdSi-δ phase is not stable at low temperature. The experimental data of Majni *et al.*[20] indicate decomposition of the PdSi-δ phase at 873 K (600 °C), while those reported by Langer and Wachetel[22] and Massara and Feschotte[12] indicate decomposition at 1097 K and 1161 K (824 °C and 888 °C), respectively. To clarify the stability of the PdSi-δ phase, the Pd-64 at. pct Si test alloy was treated at 934 K (661 °C) for 212 hours (H12 in Table II). Figure 10(a) shows the microstructure with the compositions of the phases listed in Table II. The XRD data in

UNCORRECTED PROOF

Journal : MMTA Dispatch : 28-10-2015 Pages : 15
PIPS No. : 3206 ☐ LE ☐ TYPESET
MS Code : ☐ CP ☐ DISK

Author Proof

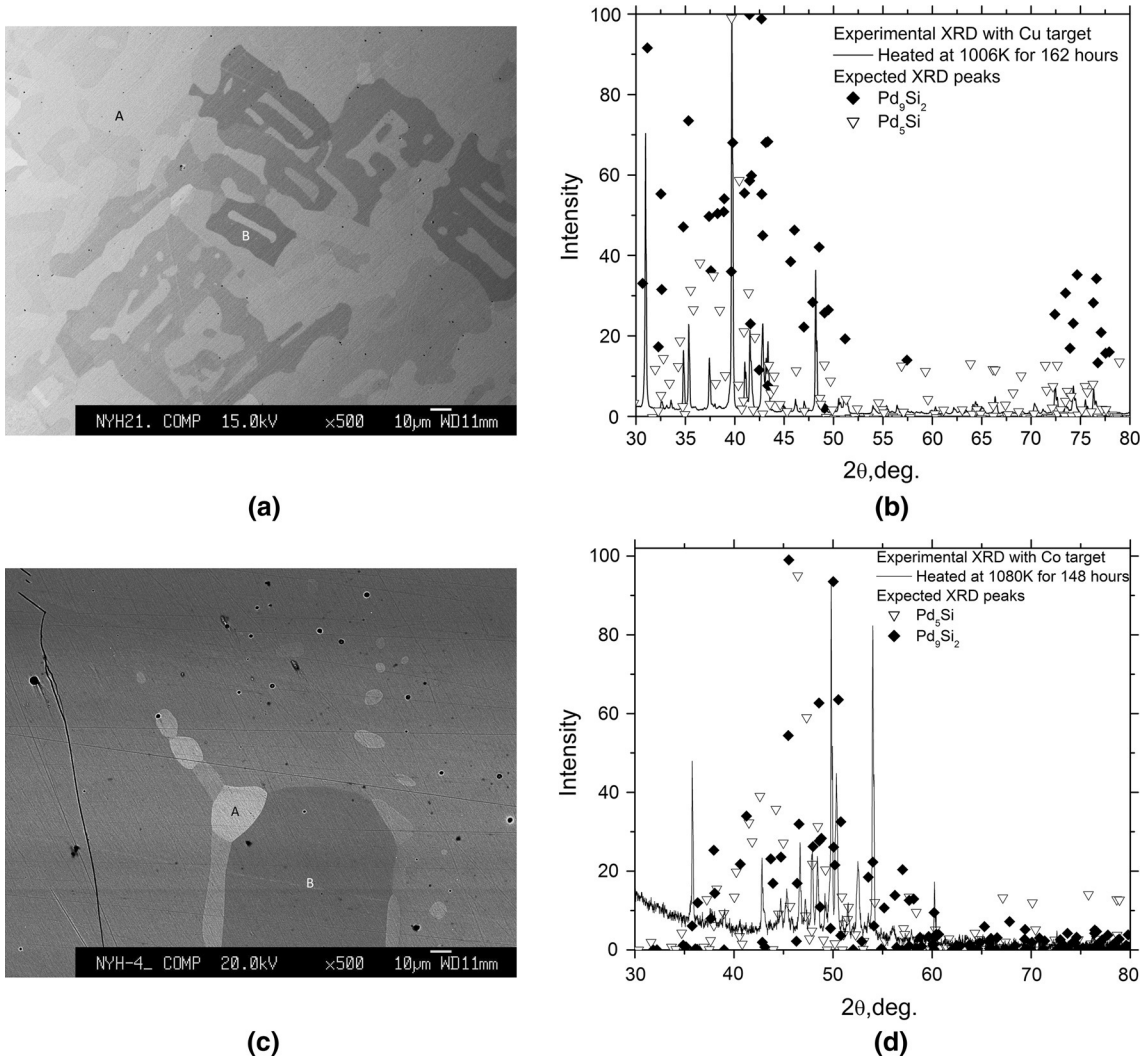

Fig. 6—(*a*) EPMA images showing observed microstructures and (*b*) the XRD data for the Pd-17 at. pct Si alloy treated at 1006 K (733 °C) for 162 h (H4) and (*c*) EPMA images showing observed microstructures and (*d*) the XRD data for the Pd-17.7 at. pct Si alloy treated at 1080 K (807 °C) for 148 h (H5). (A: Pd_5Si-μ and B: Pd_9Si_2-α).

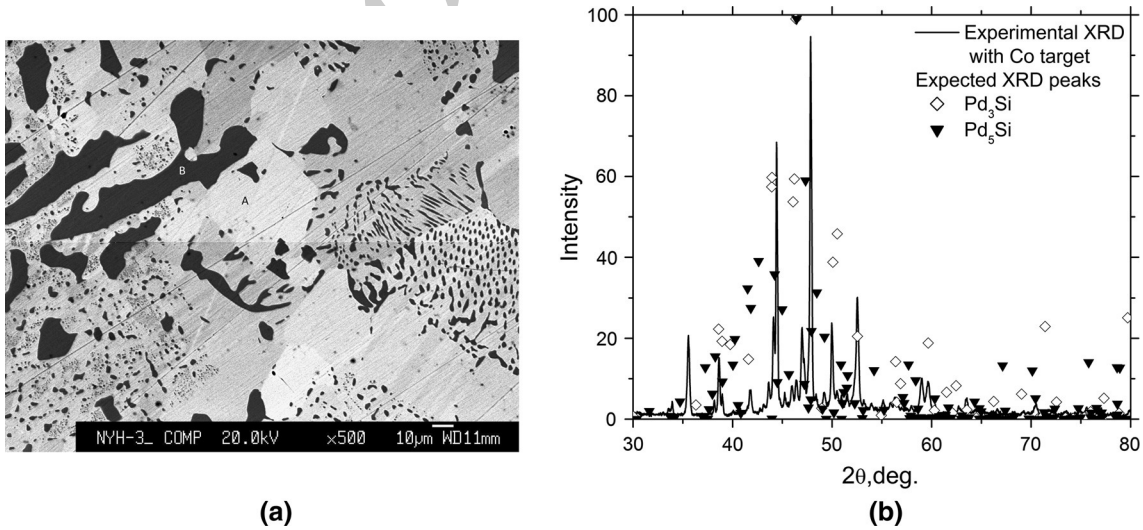

Fig. 7—(*a*) EPMA image showing observed microstructure (A: Pd_5SiSi-μ and B: Pd_3Si-β and (*b*) the XRD data for the Pd-17.7 at. pct Si alloy treated at 1093 K (820 °C) for 168 h (H6).

Journal : MMTA Dispatch : 28-10-2015 Pages : 15
PIPS No. : 3206 ☐ LE ☐ TYPESET
MS Code : ☐ CP ☐ DISK

Author Proof

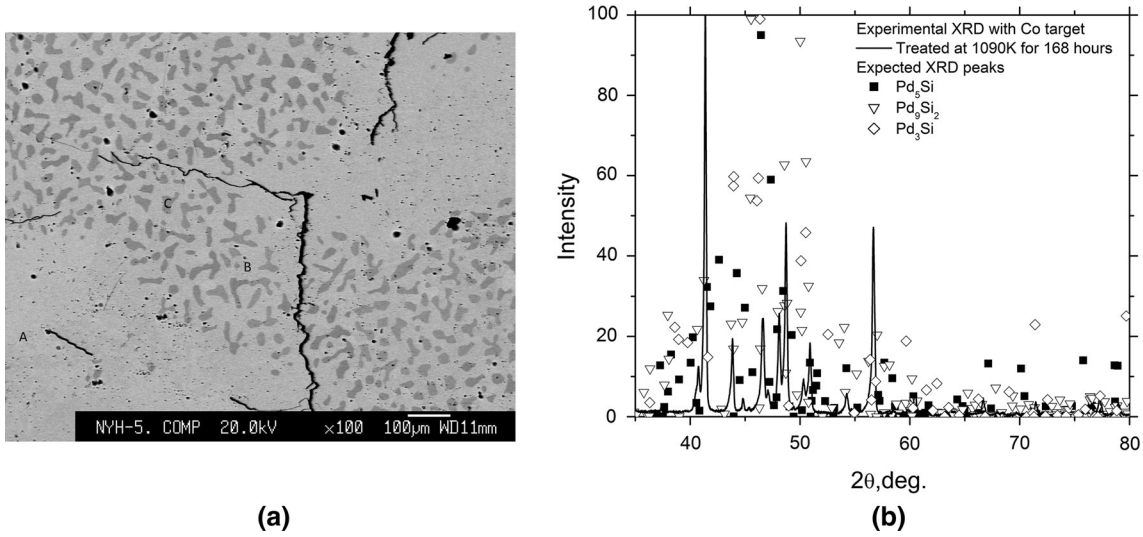

Fig. 8—(*a*) EPMA image showing observed microstructure (A: $Pd_9Si_2 - \alpha$, B: $Pd_9Si_2 - \alpha$ and C: $Pd_3Si - \beta$) and (*b*) the XRD data for the Pd-20 at. pct Si alloy treated at 1090 K (817 °C) for 168 h (H11).

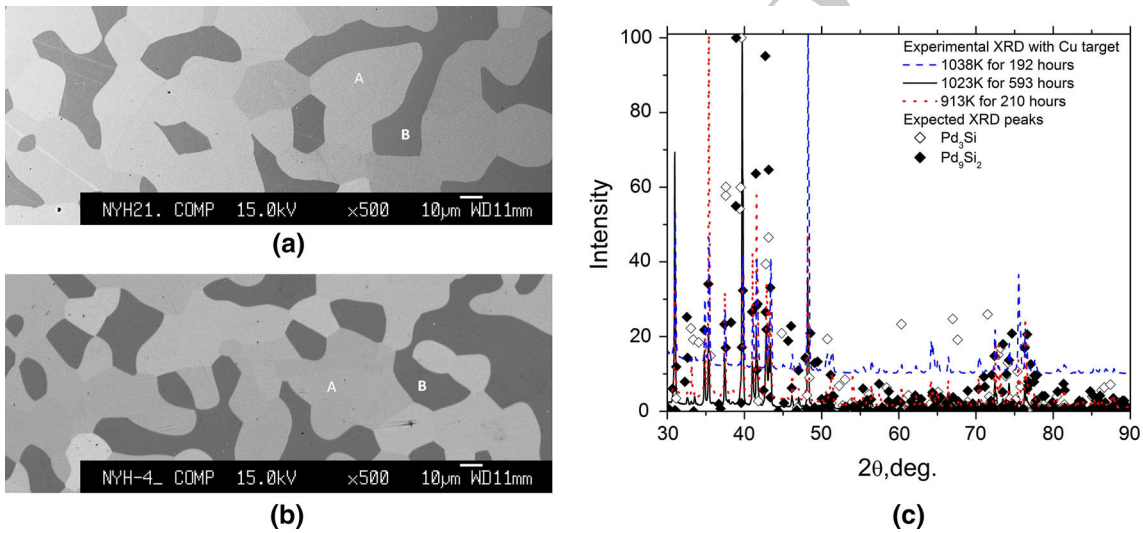

Fig. 9—EPMA image showing observed microstructure for the the Pd-20 at.pct Si alloy treated at (*a*) 913 K (640 °C) for 210 h (H7) and (*b*) 1080 K (807 °C) for 148 h (H10) (A: $Pd_9Si_2 - \alpha$ B: $Pd_3Si - \beta$) and (*c*) the XRD data for the Pd-20 at. pct Si alloy treated at different temperature (H7-9).

Figure 10(b) indicates that the phases are Pd_2Si-γ with Fe_2P prototype and Si-dia, respectively, where Si-dia is a primary phase. Therefore, we conclude that the PdSi-δ phase is not stable below 934 K (661 °C). We use the experimental report of Langer and Wachetel[22] and adopt 1097 K (824 °C) as the lower bound decomposition temperature for PdSi-δ.

According to Nylund,[24] Pd_2Si-γ exhibits the Fe_2P prototype structure. Our results in Figure 10(b) indicate that Pd_2Si-γ with the Fe_2P prototype is in equilibrium with Si-dia. To further confirm the Pd_2Si-γ phase, a Pd-31 at. pct Si test alloy was treated at 1093 K (820 °C) for 168 hours (H13 in Table II), as shown in Figure 10(c) and (d), indicating that the microstructure consists of Pd_2Si-γ and Pd_3Si-β phases. We conclude that Pd_2Si-γ is the only phase near the composition $x_{Si} = 0.333$ rather than three phases as shown in Figure 1.[11]

Based on experimental analyses and first-principles calculations discussed above, along with a review of prior reports for phase stability in this system, we treat the Pd_5Si-μ, Pd_9Si_2-α, Pd_3Si-β, Pd_2Si-γ , and PdSi-δ as stable over some temperature range and focus only on these phases in our modeling effort. With no evidence in our current study to suggest that the previously reported phases of $Pd_{14}Si_3$, $Pd_{15}Si_4$, and $Pd_{21}Si_4$-σ exhibit any range of stability and no reported structural information for any of these phases, we do not consider these phases further in the current treatment.

Journal : MMTA Dispatch : 28-10-2015 Pages : 15
PIPS No. : 3206 ☐ LE ☐ TYPESET
MS Code : ☐ CP ☐ DISK

Author Proof

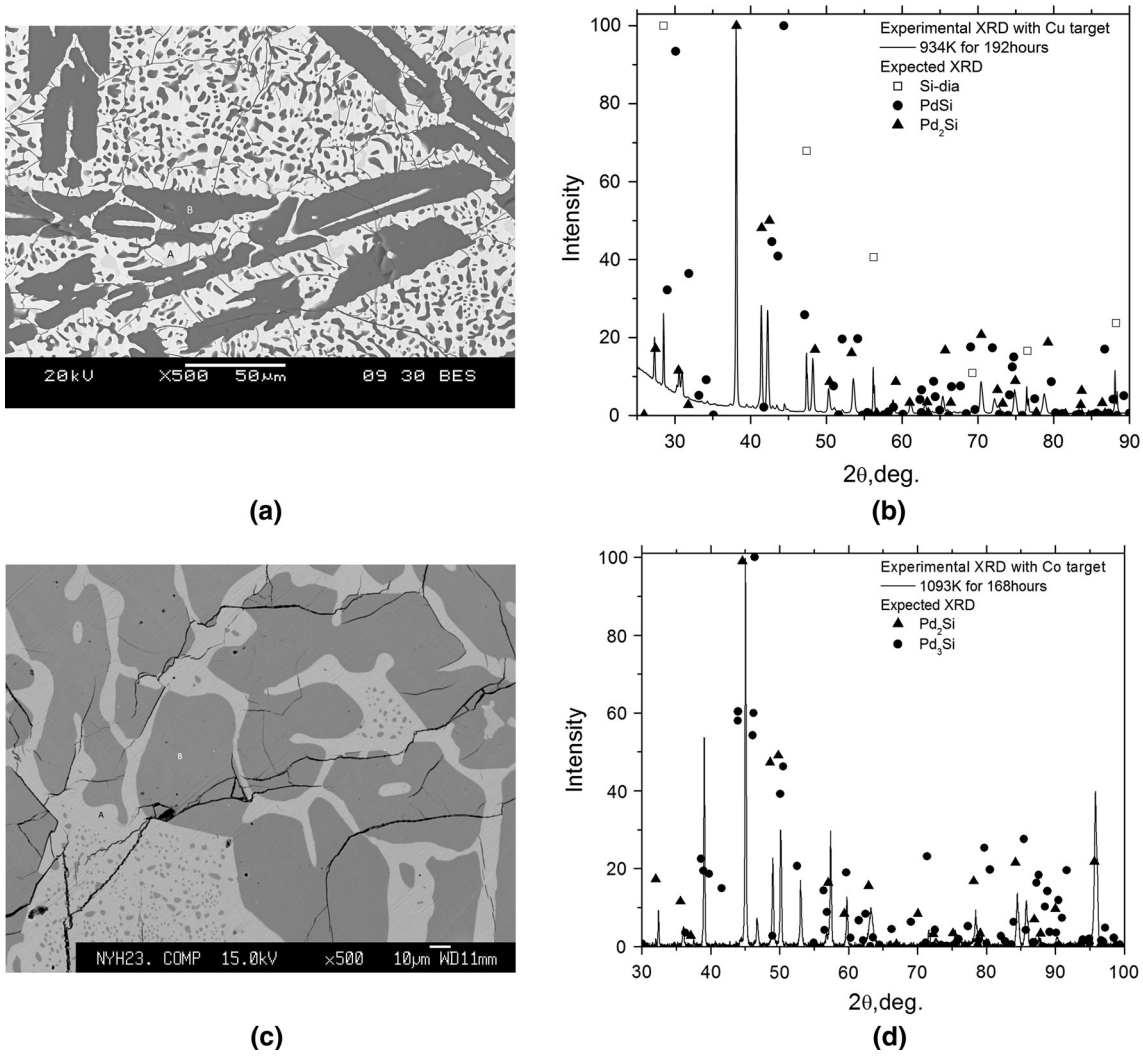

Fig. 10—(*a*) SEM image showing observed microstructure and (*b*) the XRD data for the Pd-64 at. pct Si alloy treated at 934 K (661 °C) for 212 h (H12) (A: Pd_2Si-γ B: *Si*) . (*c*) EPMA image showing observed microstructure and (*d*) the XRD data for the Pd-31 at. pct Si alloy treated at 1093 K (820 °C) for 168 h (H13) (A: Pd_3Si-β B: Pd_2Si-γ).

IV. ENERGETICS AND RESULT ANALYSIS

The binary Pd-Si binary phase diagram is described here using a standard semi-empirical solution-based modeling approach, incorporating experimental data and first-principles calculations for parameter evaluation. A total of 8 distinct phases are included in the current description, as listed in Table IV, where the liquid phase is described with the association model, and the fcc and Si-dia phases are modeled as binary regular solutions, and the five intermediate phases (Pd_5Si-μ, Pd_9Si_2-α, Pd_3Si-β, Pd_2Si-γ, and PdSi-δ) are treated with a two-sublattice model. For any phase, ϕ, the total Gibbs free energy is given generally by the sum of three contributions:

$$G_m^{\phi} = {}^{ref}G_m^{\phi} + {}^{id}G_m^{\phi} + {}^{xs}G_m^{\phi}, \qquad [2]$$

where the subscript, m, indicates that all terms are molar quantities. The first term in Eq. [2] is the sum of occupancy-weighted sublattice end-member contributions, while the second and third terms are the ideal and excess parts of the Gibbs free energy of mixing, respectively. The comprehensive thermodynamic model is detailed in Table IV while the parameters for end-member properties from Reference 32 and mixing properties are given in Tables V and VI, respectively. Parameter evaluation is based on experimental data and first-principles results, as described briefly below.

The parameter evaluation process was begun by considering the liquid phase. Based on reported chemical short-range ordering (CSRO) centered around the Pd_2Si composition,[33] we choose to formulate the solution free energy using three chemical associate species, including Pd, Si, and Pd_2Si. Additionally, the high melting temperature of the Pd_2Si phase demonstrates its high relative stability, and this composition is consistent with a minimum in the measured enthalpy of

Journal : MMTA Dispatch : 28-10-2015 Pages : 15
PIPS No. : 3206 ☐ LE ☐ TYPESET
MS Code : ☐ CP ☐ DISK

Table IV. Summary of the Thermodynamic Models Used for the Pd-Si Binary System

Phase	Prototype	Model (Formulation)	Model
Liquid			${}^{\text{ref}}G_{\text{m}}^{\text{liq}} = \frac{1}{1+2y_{\text{Pd}_2\text{Si}}}\sum_{i=\text{Pd,Pd}_2\text{Si,Si}} y_i {}^0G_i^{\text{liq}}$
			${}^0G_{\text{Pd}_2Si}^{\text{liq}} = (2{}^0G_{\text{Pd}}^{\text{liq}} + {}^0G_{\text{Si}}^{\text{liq}} + \Delta G^0_{\text{Pd}_2Si})$
		association model	${}^{\text{id}}G_{\text{m}}^{\text{liq}} = \frac{RT}{1+2y_{\text{Pd}_2\text{Si}}}\sum_i y_i \ln y_i$
		$(\text{Pd}, \text{Pd}_2\text{Si}, \text{Si})$	${}^{xs}G_{\text{m}}^{\text{liq}} = \frac{1}{1+2y_{\text{Pd}_2\text{Si}}}\sum_i \sum_{j>i} y_i y_j {}^0L_{i,j}^{\text{liq}}$
			$(i,j = \text{Pd}, \text{Pd}_2\text{Si}, \text{Si})$
			y_i is mole fraction of species i
Pd-fcc	Cu	solution model	${}^{\text{ref}}G_{\text{m}}^{\Phi} = \sum_{i=\text{Pd,Si}} x_i {}^0G_i^{\Phi}$
Si-dia	C		${}^{\text{id}}G_{\text{m}}^{\Phi} = RT\sum_{i=\text{Pd,Si}} x_i ln x_i$
			${}^{xs}G_{\text{m}}^{\Phi} = x_{\text{Pd}}x_{\text{Si}}\sum_{k=0} {}^jL_{\text{Pd,Si}}^{\Phi}(x_{\text{Pd}} - x_{\text{Si}})^k$
Two-sublattice model $(\text{Pd}, \text{Si})_p(\text{Pd}, \text{Si})_q$			
Pd_9Si_2-α	Pd_9Si_2	$(\text{Pd}, \text{Si})_{.818}(\text{Pd}, \text{Si})_{.182}$	${}^{\text{ref}}G_{\text{m}}^{\Phi} = \sum_{i=\text{Pd,Si}} y_i^{\text{I}} \sum_{i=\text{Pd,Si}} y_i^{\text{II}} {}^0G_{i:j}^{\Phi}$
Pd_3Si-β	Fe_3C	$(\text{Pd}, \text{Si})_{0.75}(\text{Pd}, \text{Si})_{0.25}$	${}^0G_{i:j}^{\Phi} = \Delta G_{i:j}^{\Phi} + p{}^0G_i^{\text{ref}} + q{}^0G_j^{\text{ref}}$
Pd_2Si-γ	Fe_2P	$(\text{Pd}, \text{Si})_{0.667}(\text{Pd}, \text{Si})_{0.333}$	${}^{\text{id}}G_{\text{m}}^{\Phi} = RT\sum_{i=\text{Pd,Si}} (py_i^{\text{I}} \ln y_i^{\text{I}} + qy_i^{\text{II}} \ln y_i^{\text{II}})$
PdSi-δ	MnP	$(\text{Pd}, \text{Si})_{0.5}(\text{Pd}, \text{Si})_{0.5}$	${}^{xs}G_{\text{m}}^{\Phi} = y_{\text{Pd}}^{\text{I}}y_{\text{Si}}^{\text{I}}\sum_{i=\text{Pd,Si}} y_i^{\text{II}}\sum_{k=0} {}^jL_{\text{Pd,Si:}i}^{\Phi}(y_{\text{Pd}}^{\text{I}} - y_{\text{Si}}^{\text{I}})^k$
Pd_5Si-μI	Pd_5P	$(\text{Pd}, \text{Si})_{0.833}(\text{Pd}, \text{Si})_{0.167}$	$+y_{\text{Pd}}^{\text{II}}y_{\text{Si}}^{\text{II}}\sum_{i=\text{Pd,Si}} y_i^{\text{I}}\sum_{k=0} {}^jL_{i:\text{Pd,Si}}^{\Phi}(y_{\text{Pd}}^{\text{II}} - y_{\text{Si}}^{\text{II}})^k$
Pd_5Si-μII			${}^0G_{\text{Pd}}^{\text{ref}} = {}^0G_{\text{Pd}}^{\text{fcc}};\ {}^0G_{\text{Si}}^{\text{ref}} = {}^0G_{\text{Si}}^{\text{dia}}$
Pd_5Si-μIII		$(\text{Pd}, \text{Si})_{0.84}(\text{Pd}, \text{Si})_{0.16}$	

mixing, as shown in Figure 11. With these experimental data,[33–37] the model parameters for liquid in Table IV were evaluated, as listed in Table VI. The corresponding model values for mixing properties (enthalpy and Gibbs free energy) are shown in Figures 11(a) and (b) and compared with experimental reports of mixing enthalpy at 1400 K, 1600 K, 1723 K, and 1820 K (1127 °C, 1327 °C, 1450 °C, and 1547 °C).* The equilibrium associate fractions varying with composition (at 1700 K (1427 °C)) and over a range of temperature (with $x_{\text{Si}} = 0.33$) are shown in Figures 11(c) and (d), respectively, where the equilibrium fraction of Pd_2Si increases with decreasing temperature.

The Pd-fcc and Si-dia phases are treated as simple binary substitutional solutions. The parameters for the fcc phase were evaluated using reported experimental data,[19–22,40] as listed in Table VI. The end-member ${}^0G_{\text{Pd}}^{\text{dia}}$ listed in Table VI is described as ${}^0G_{\text{Pd}}^{\text{fcc}} + (E_{\text{Pd}}^{\text{dia}} - E_{\text{Pd}}^{\text{fcc}})$, where the E^{ϕ} values are computed from first-principles, as listed in Table I.

Each intermetallic phase (Pd_5Si-μ, Pd_9Si_2-α, Pd_3Si-β, Pd_2Si-γ, and PdSi-δ) is described as a two-sublattice solid solution with the form $(\text{Pd}, \text{Si})_p(\text{Pd}, \text{Si})_q$, such that there are four solution end members, with a free energy given by ${}^0G_{i:j}^{\phi}$. For each of these end-member energies, the associated Gibbs free energy of formation, $\Delta G_{i:j}^{\phi}$ (i,j = Pd,Si), for each relevant sublattice end-members (Pd_pPd_q, Pd_pSi_q, Si_pPd_q, and Si_pSi_q) is described as $a_{i:j}^{\phi} + b_{i:j}^{\phi}T + c_{i:j}^{\phi}T\ln T$. These phases are discussed below individually and the parameters are tabulated in Table VI.

For the Pd_2Si-γ phase, the four parameters, $a_{i:j}^{\gamma}$ (i,j = Pd,Si) in Table VI, are determined with the first-principles results in Table I. With the experimental melting temperature in Figure 12(a), the parameter $b_{\text{Pd:Si}}^{\gamma}$ is determined in Table VI, while the remainder parameters ($b_{\text{Pd:Pd}}^{\gamma}$, $b_{\text{Si:Pd}}^{\gamma}$, $b_{\text{Si:Si}}^{\gamma}$ and $c_{i:j}^{\gamma}$) for the end member of the γ phase were assumed to be zero. The interaction parameter ${}^0L_{\text{Pd,Si:Si}}^{\gamma}$ was considered to describe the homogeneous range of the γ phase and evaluated with experimental data.[12,22]

Similar to the γ phase, the parameters $a_{i:j}^{\beta}$ (i,i = Pd,Si) for the Pd_3Si-β phase are determined with the first-principles data in Table I. If we just employ the parameter $b_{\text{Pd:Si}}^{\beta}$ which is determined with melting temperature[10,12,19,20,22,23] and set the parameter $c_{\text{Pd:Si}}^{\beta}$ to be

*Enthalpy of mixing results in Ref. [38,39] mentioned in Ref. [11] were not implemented in the present analysis. The calorimeter measurements reported in Ref. [38] are for the Cu-In system rather than the Pd-Si system. In Ref. [39], the enthalpy of mixing for Pd-Si liquid was calculated from the partial enthalpies of Pd and Si using the Gibbs-Duhem relation rather than direct measurement. As authors mentioned in the report,[39] the calculated partial enthalpy of Si does not quite agree with the experimental ones. Therefore, instead of results in Ref. [39], we plotted the experimental data[35,37] measured more recently (by the same group as Ref. [39] in Figure 11(a).)

Author Proof

UNCORRECTED PROOF

Journal : MMTA Dispatch : 28-10-2015 Pages : 15
PIPS No. : 3206 LE TYPESET
MS Code : CP DISK

Table V. Coefficients for the Standard Gibbs Free Energies of Pure Pd and Si Elements in the Relevant Phases

	${}^0G_{\mathrm{Pd}}^{\mathrm{liq}}$			${}^0G_{\mathrm{Pd}}^{\mathrm{fcc}}$		
$T_{\min}$K(°C)	298 (25)	600 (327)	1828 (1555)	298 (25)	900 (627)	1828 (1555)
$T_{\max}$K(°C)	600 (327)	1828 (1555)	4000 (3727)	900 (627)	1828 (1555)	4000 (3727)
${}^0G_i^{\mathrm{ref}}$	—	—	—	—	—	—
a_0	1303.037	23,392.81	−12,375.903	−10,204.027	917.062	−67,256.956
a_1	170.965792	−116.745522	251.420646	176.076315	49.659893	370.497818
a_2	−32.211	10.8666189	−41.17	−32.211	−13.5708	−54.2560279
$a_3 \times 10^2$	0.7120975	−2.7246584	—	0.7120975	−0.717522	0.021017
$a_4 \times 10^6$	−1.919875	2.428271	—	−1.919875	0.191115	−0.063199
$a_5 \times 10^{21}$	—	—	—	—	—	—
a_6	168,687	−1,852,450	—	168,687	−1,112,465	18,715,959
$a_7 \times 10^{-30}$	—	—	—	—	—	—

	${}^0G_{\mathrm{Pd}}^{bcc}$	${}^0G_{\mathrm{Pd}}^{hcp}$	${}^0G_{\mathrm{Si}}^{\mathrm{dia}}$		${}^0G_{\mathrm{Si}}^{\mathrm{liq}}$	
$T_{\min}$K(°C)	298 (25)	298 (25)	298 (25)	1687 (1414)	298 (25)	1687 (1414)
$T_{\max}$K(°C)	4000 (3727)	4000 (3727)	1687 (1414)	3600 (3327)	1687 (1414)	3600 (3327)
${}^0G_i^{\mathrm{ref}}$	${}^0G_{\mathrm{Pd}}^{\mathrm{fcc}}$	${}^0G_{\mathrm{Pd}}^{\mathrm{fcc}}$	—	—		
a_0	10500	2000	−8162.609	−9457.642	50,696.36	49,828.165
a_1	−1.8	0.1	137.227259	167.271767	−30.099439	−29.559068
a_2	—	—	−22.8317533	−27.196	—	—
$a_3 \times 10^2$	—	—	−0.1912904	—	—	—
$a_4 \times 10^6$	—	—	—	—	—	—
$a_5 \times 10^{21}$	—	—	—	—	2.0931	—
a_6	—	—	176,667	—	—	—
$a_7 \times 10^{-30}$	—	—	—	—	—	4.2037

	${}^0G_{\mathrm{Si}}^{\mathrm{fcc}}$
$T_{\min}$K(°C)	298 (25)
$T_{\max}$K(°C)	3600 (3327)
${}^0G_{\mathrm{Si}}^{\theta}$	$5100 - 21.8\mathrm{T} + {}^0G_{\mathrm{Si}}^{\mathrm{dia}}$

Each Gibbs free energy is described as ${}^0G_i^{\theta} = {}^0G_i^{\mathrm{ref}} + a_0 + a_1T + a_2TlnT + a_3T^2 + a_4T^3 + a_5T^7 + a_6T^{-1} + a_7T^{-9}$.[32]

zero, the calculated liquidus deviates from the experimental data.[10,12,19,20,22,23] The parameter $c_{\mathrm{Pd:Si}}^{\beta}$ thus has to be considered and is evaluated in Table VI. The remainder parameters were assumed to be zero.

As description in Section II, the first-principles result indicates that the Pd_5Si-μ phase with the composition 16.7 at. pct Si is stable at zero kelvin, while the experimental data in Section III show that the composition of the Pd_5Si-μ phase is between 16 and 16.3 at. pct Si at high temperature. First-principles calculation were not performed for the Pd_5Si-μ phase with the composition at 16 at. pct Si due to unclear atomic configuration. For prospective application, the Pd_5Si-μ phase thus is described with the two formulations, $(\mathrm{Pd,Si})_{0.833}(\mathrm{Pd,Si})_{0.167}$ and $(\mathrm{Pd,Si})_{0.84}(\mathrm{Pd,Si})_{0.16}$, respectively. Three parameter sets were evaluated for the Pd_5Si-μ phase for the formulations (1) $(\mathrm{Pd,Si})_{0.833}(\mathrm{Pd,Si})_{0.167}$ marked as μI in which the interaction parameter is not considered; (2) $(\mathrm{Pd,Si})_{0.833}(\mathrm{Pd,Si})_{0.167}$ marked as μII with considering interaction parameters; and (3) $(\mathrm{Pd,Si})_{0.84}$ $(\mathrm{Pd,Si})_{0.16}$ marked as μIII with considering interaction parameters. The parameters $a_{i:j}^{\mu k}$ (k = I, II, and III) of the end members except $a_{\mathrm{Pd:Si}}^{\mu\mathrm{III}}$ are estimated with the first-principles data in Table I. $a_{\mathrm{Pd:Si}}^{\mu\mathrm{III}}$ was assumed to be equal to the value at $x_{\mathrm{Si}} = 0.16$ on the linear combination between $\Delta H^{\mathrm{fcc}}(=0)$ and $\Delta H_{f(\mathrm{Pd_5Si})}^{\mu}$ from the data in Table I as the dash-line in Figure 2. The parameter $b_{\mathrm{Pd:Si}}^{\mu}$ is determined with the melting temperature in Tables II and III. As shown in Figure 12(b), the calculated phase diagram shows eutectoid and following peritectoid reactions for the Pd_5Si-μ phase. According to the conclusion in Section III, Pd_5Si-μ is stable all way to zero temperature. The parameter $c_{\mathrm{Pd:Si}}^{\mu}$ thus has to be employed. The interaction parameters ${}^iL_{\mathrm{Pd:Pd,Si}}^{\mu\mathrm{II}}$ and ${}^iL_{\mathrm{Pd,Si:Si}}^{\mu\mathrm{III}}$ of the Pd_5Si-μ phase were determined with the composition data in Table II. The evaluated parameters are listed Table VI. The three parameter sets for the Pd_9Si_2-α phase correspond to each of three parameter sets for the Pd_5Si-μ phase (I, II, III) and are evaluated with the data in Table I and Section III. Figures 12(cI) through (cIII) are the calculated phase diagrams using the three parameter sets for the Pd_5Si-μ and Pd_9Si_2-α phases in Tables V and VI, respectively.

The PdSi-δ phase is a high temperature stable phase, and its parameters $a_{\mathrm{Pd:Si}}^{\delta}$ and $b_{\mathrm{Pd:Si}}^{\delta}$ were evaluated with the melting temperature and decomposition reaction PdSi-$\delta \rightarrow Pd_2Si$-$\gamma + Si$ at 1097 K (824 °C). The parameters $a_{i:j}^{\delta}$ ($i:j = \mathrm{Pd:Pd}$, $Si:Pd$ and $Si:Si$) are

Author Proof
UNCORRECTED PROOF

Journal : MMTA Dispatch : 28-10-2015 Pages : 15
PIPS No. : 3206 LE TYPESET
MS Code : CP DISK

Table VI. Thermodynamic Model Parameters (in SI Unit)

Phase	Parameter	Value(J/mol)
Liquid	${}^{0}L^{liq}_{Pd,Si}$	−105,332
	${}^{0}L^{liq}_{Pd,Pd_2Si}$	−63,365
	${}^{0}L^{liq}_{Pd_2Si,Si}$	−41,233
	$\Delta G^{0}_{Pd_2Si}$	−258,603 + 77.632T
fcc	${}^{0}L^{fcc}_{Pd,Si}$	−267,130 + 84.465T
	${}^{1}L^{fcc}_{Pd,Si}$	−6500
dia	${}^{0}G^{dia}_{Pd}$	109,648.6 + ${}^{0}G^{fcc}_{Pd}$
Pd_9Si_2-α	$\Delta G^{\alpha}_{Pd:Pd}$	34,454.45
	$\Delta G^{\alpha}_{Pd:Si}$ to μI	−42,757.3 + 1.16864Tln(T) − 1.3993T
	$\Delta G^{\alpha}_{Pd:Si}$ to μII	−42,757.3 + 1.2991Tln(T) − 2.3023T
	$\Delta G^{\alpha}_{Pd:Si}$ to μIII	−42,757.3 + 3.6842Tln(T) − 18.9845T
	$\Delta G^{\alpha}_{Si:Pd}$	36,649.54
	$\Delta G^{\alpha}_{Si:Si}$	62,418.91
Pd_3Si-β	$\Delta G^{\beta}_{Pd:Pd}$	30,162.83
	$\Delta G^{\beta}_{Pd:Si}$	−57,900 − 15.23186T + 3.47175Tln(T)
	$\Delta G^{\beta}_{Si:Pd}$	10,600
	$\Delta G^{\beta}_{Si:Si}$	1880
Pd_2Si-γ	$\Delta G^{\gamma}_{Pd:Pd}$	186,725.7
	$\Delta G^{\gamma}_{Pd:Si}$	−65,242.5 + 10.318T
	$\Delta G^{\gamma}_{Si:Pd}$	169,447.37
	$\Delta G^{\gamma}_{Si:Si}$	148,096.3
	${}^{0}L^{\gamma}_{Pd,Si:Si}$	−131,909.17
PdSi-δ	$\Delta G^{\delta}_{Pd:Pd}$	35,931.5
	$\Delta G^{\delta}_{Pd:Si}$	−35,329.5 − 4.777T
	$\Delta G^{\delta}_{Si:Pd}$	43,170
	$\Delta G^{\delta}_{Si:Si}$	45,978.5
	${}^{0}L^{\delta}_{Pd,Si:Si}$	−24,978.5
Pd_5Si-μI	$\Delta G^{\mu}_{Pd:Pd}$	48,686.6
	$\Delta G^{\mu}_{Pd:Si}$	−39,441 + 0.69Tln(T) + 1.430644342T
	$\Delta G^{\mu}_{Si:Pd}$	43,174.59
	$\Delta G^{\delta}_{Si:Si}$	66,394.6
Pd_5Si-μII	$\Delta G^{\mu}_{Pd:Pd}$	48,686.6
	$\Delta G^{\mu}_{Pd:Si}$	−39,441 + 0.865Tln(T) + 0.31036T
	$\Delta G^{\mu}_{Si:Pd}$	43,174.59
	$\Delta G^{\mu}_{Si:Si}$	66,394.6
	${}^{0}L^{\mu}_{Pd:Pd,Si}$	−33,546
	${}^{1}L^{\mu}_{Pd:Pd,Si}$	14,546
Pd_5Si-μIII	$\Delta G^{\mu}_{Pd:Pd}$	48,686.6
	$\Delta G^{\mu}_{Pd:Si}$	−38,000 + 2.66Tln(T) − 12.409T
	$\Delta G^{\mu}_{Si:Pd}$	43,174.59
	$\Delta G^{\mu}_{Si:Si}$	66,394.6
	${}^{0}L^{\mu}_{Pd,Si:Si}$	−73,546
	${}^{1}L^{\mu}_{Pd,Si:Si}$	−140,546

Author Proof
UNCORRECTED PROOF

Journal : MMTA Dispatch : 28-10-2015 Pages : 15
PIPS No. : 3206 ☐ LE ☐ TYPESET
MS Code : ☐ CP ☐ DISK

Author Proof

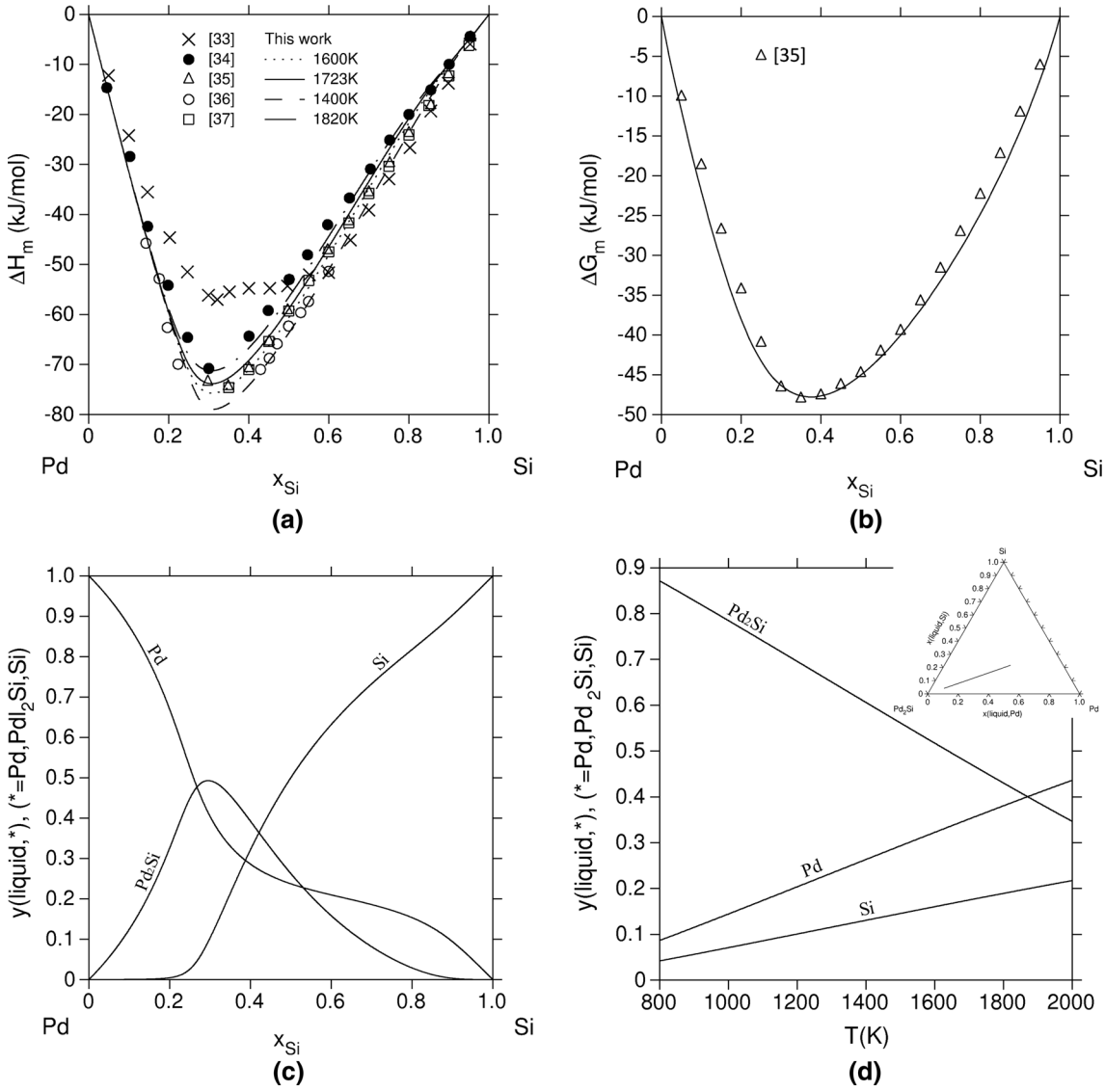

Fig. 11—(*a*) The enthalpy of mixing; (*b*) Gibbs free energy of mixing (at 1723 K (1450 °C)); (*c*) the calculated associate species fraction *vs* composition (at 1723 K (1450 °C)) and (*d*) temperature dependence (at $x_{Si} = 0.33$) of the associate species fraction of the liquid phase as computed using the present model in Tables V and VI.

determined with the first-principles data in Table I, while the parameters $b^{\delta}_{i:j}$ and $c^{\delta}_{i:j}$ are assumed to be zero. The interaction parameter ${}^{0}L^{\delta}_{Pd:Pd,Si}$ was evaluated with experimental data,[12] *i.e.*, liquid→PdSi-δ + *Si*.

The reliability of this evaluation arises from the use of both first-principles calculations and experiments to clarify the relative stability of the intermetallic phases. Our findings show several significant differences in comparison with previous report.[9,11] Notably, (i) the calculated enthalpies of formation (solid line) for the compounds shown in Figure 12 and the experimental data in Table II indicate that Pd_5Si-μ, Pd_9Si_2-α, Pd_3Si-β, and Pd_2Si-γ are stable all the way to zero Kelvin, while PdSi-δ decomposes into other phases at low temperature. The $Pd_{21}Si_4$-σ, $Pd_{14}Si_3$, and $Pd_{15}Si_4$, being not observed in our experimental measurements, are not considered as stable phases in thermodynamic modeling. (ii) The fcc phase boundary shows good agreement with experimental data (Figure 12(a)). (iii) Pd_3Si-β is described as congruent melting compound. (iv) The compounds Pd_2Si, Pd_2Si-I and Pd_2Si-II shown in Figure 1[11] are described as one phase, *i.e.*, Pd_2Si-γ with homogeneous composition range. The calculated thermodynamic properties and phase diagram from the model are shown in Figures 2, 11, and 12, where we can see that the experimental data and first-principles data are well represented.

V. SUMMARY

The stabilities of the compounds in Pd-Si system were investigated by employing first-principles calculations and experimental measurements. The results indicate

Journal : MMTA Dispatch : 28-10-2015 Pages : 15
PIPS No. : 3206 ☐ LE ☐ TYPESET
MS Code : ☐ CP ☐ DISK

Author Proof

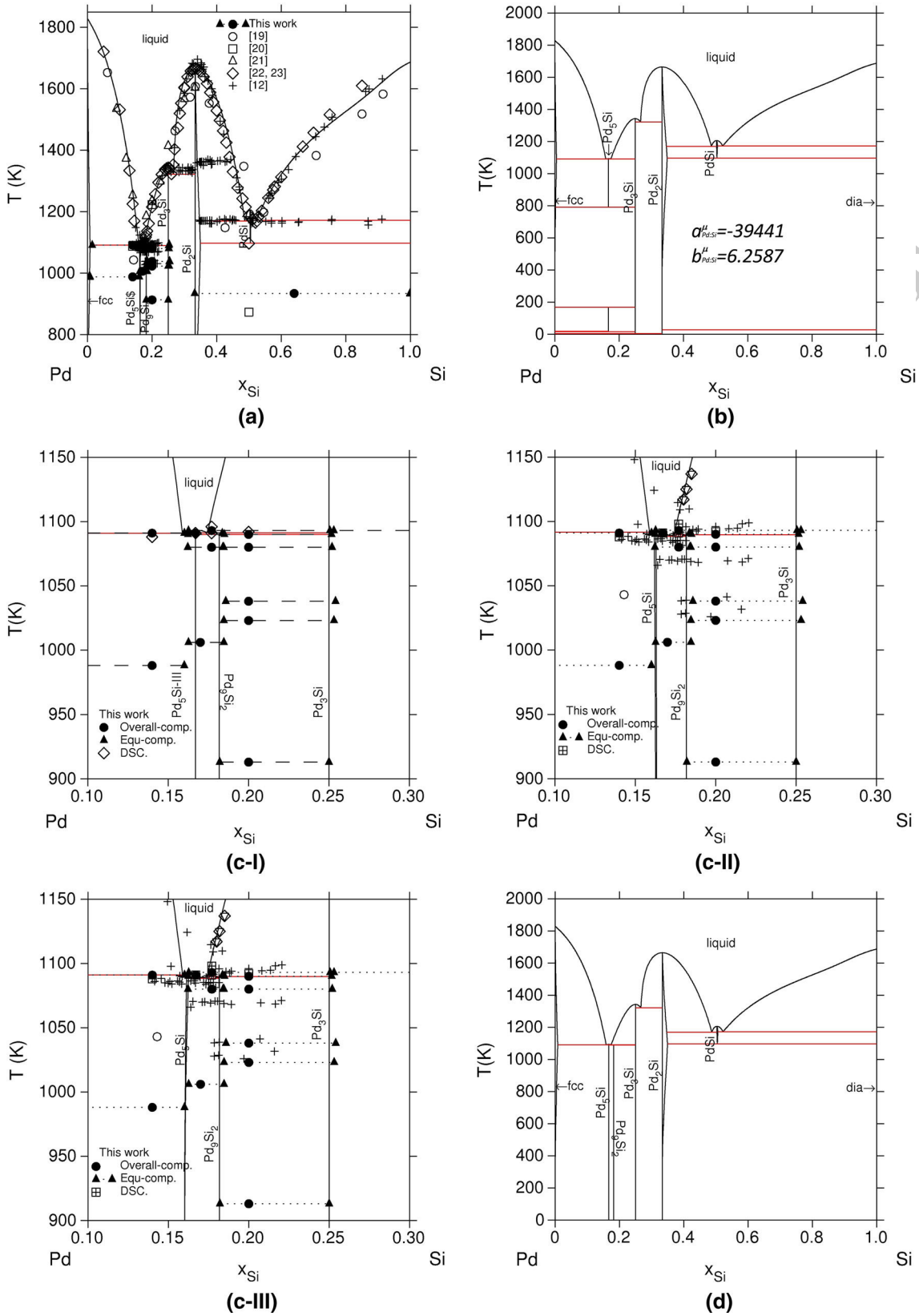

Fig. 12—Pd-Si phase diagram computed with the present model (as listed in Tables V, VI): (*a*) plotted for comparison with experimental data; (*b*) optimized for $c^{\mu}_{Pd:Si}=0$, as listed in the figure; (*c*) showing three results corresponding to three parameter sets for μ (I, II, III); and (*d*) the equilibrium phase diagram (same as (a)) without the experimental data.

Journal : MMTA Dispatch : 28-10-2015 Pages : 15
PIPS No. : 3206 ☐ LE ☐ TYPESET
MS Code : ☐ CP ☐ DISK

that the Pd_5Si-μ, Pd_9Si_2-α, Pd_3Si-β, and Pd_2Si-γ are stable all way to zero temperature, while PdSi-δ is a high temperature stable phase. The $Pd_{21}Si_4$-σ, $Pd_{14}Si_3$, and $Pd_{15}Si_4$ phases were not observed in our experiments and are not considered as stable phases. Due to component Si dissolved in Pd-fcc and Pd in Si-dia, the lattice parameters of the Pd-fcc phase in the heat-treated Pd-14 at. pct Si alloy and the Si-dia phase in the heat-treated Pd-64 at. pct Si alloy deviate from those of pure elements. In the thermodynamic treatment, the model parameters are fitted using available experimental data and first-principles data, and the resulting phase diagram is reported over the full range of compositions in the Pd-Si binary system.

ACKNOWLEDGMENTS

This work was supported by the U.S. Department of Energy (DOE), Office of Science, Basic Energy Sciences, Materials Science and Engineering Division. The research was performed at the Ames Laboratory, which is operated for the U.S. DOE by Iowa State University under contract No. DE-AC02-07CH11358.

REFERENCES

1. *Integrated Computational Materials Engineering*, The National Academies Press, Washington, DC, 2008.
2. S.H. Zhou and R.E. Napolitano: *Acta Mater.*, 2006, vol. 54, pp. 831–40.
3. S.H. Zhou and R.E. Napolitano: *J. Phase Equilib.*, 2007, vol. 28, pp. 328–34.
4. S.H. Zhou and E.R. Napolitano: *Phys. Rev. B:*, 2008, vol. 78, p. 148111.
5. K.F. Yao and R. Fang: *Chin. Phys. Lett.*, 2005, vol. 22, pp. 1481–83.
6. H.S. Chen, L.C. Kimerling, J.M. Poate, and W.L. Brown: *Appl. Phys. Lett.*, 1978, vol. 23, p. 461.
7. S.T.J. Steinberg and A.E. Lord: *Appl. Phys. Lett.*, 1981, vol. 38, p. 878.
8. H.Y. Ding, Y. Li, and K.F. Yao: *Chin. Phys. Lett.*, 2010, vol. 27, p. 126101.
9. N. Saunders: *CALPHAD*, 1985, vol. 9, pp. 297–309.
10. H.C. Baxi and T.B. Massalski: *J. Phase Equilib.*, 1991, vol. 12, pp. 349–56.
11. Z.M. Du, X.J. Yang, C.P. Guo, and T. Liu. *Intermetallics*, 2006, vol. 14, pp. 560–69.
12. R. Massara and P. Feschotte: *J. Alloys Compd.*, 1993, vol. 190, pp. 249–54.
13. P. Duhaj and P. Svec: *Mater. Sci. Eng. A*, 1997, vols. 226–228, pp. 245–54.
14. K.L. Lee and H.W. Kui: *J. Mater. Res.*, 1999, vol. 14, pp. 3653–62.
15. K.L. Lee and H.W. Kui: *J. Mater. Res.*, 1999, vol. 14, pp. 3663–67.
16. S.Y. Hong, W.H. Gue, and H.W. Kui: *J. Mater. Res.*, 1999, vol. 14, pp. 3668–72.
17. P. Mrafko, P. Duhaj, P. Svec, and J. Non-Cryst: *Solids*, 2006, vol. 352, pp. 5284–86.
18. P. Chen, K.-F. Yao, and F. Ruan: *Philos. Mag. Lett.*, 2007, vol. 87, pp. 677–86.
19. N.K. Rao and H. Winterhager: *Trans. Indian Inst. Met.*, 1956, vol. 10, pp. 139–42.
20. G. Majni, F. Nava, G. Ottaviani, E. Danna, G. Leggieri, A. Luches, and G. Celotti: *J. Appl. Phys.*, 1981, vol. 52, pp. 4055–61.
21. J.A. Wysocki and P.E. Duwes: *Metall. Mater. Trans. A*, 1981, vol. 12A, pp. 1455–60.
22. H. Langer and E.Z. Wachetel: *Z. Metallkd.*, 1981, vol. 72, pp. 769–75.
23. H. Langer and E.Z. Wachetel: *Z. Metallkd.*, 1983, vol. 74, pp. 535–44.
24. A. Nylund: *Acta Chem. Scand.*, 1966, vol. 20, pp. 2381–86.
25. S.V. Meschel and O.J. Kleppa: *J. Alloys Compd.*, 1998, vol. 274, pp. 193–200.
26. T.G. Chart: *High Temp. High Press*, 1973, vol. 5, pp. 241–51.
27. A. Pasturel, P. Hicter, and F. Cyrot-lackmann: *Physica*, 1984, vol. 120B, pp. 247–50.
28. G. Kresse and D. Joubert: *Phys. Rev. B*, 1999, vol. 59, pp. 1758–75.
29. P.E. Blöchl: *Phys. Rev. B*, 1994, vol. 50, pp. 17953–79.
30. J.P. Perdew, K. Burke, and M. Ernzerhof: *Phys. Rev. B*, 1996, vol. 77, pp. 3865–68.
31. MPC: Materials Preparation Center, Ames Laboratory, Ames, IA.
32. A.T. Dinsdale: *CALPHAD*, 1991, vol. 4, pp. 317–425.
33. N.A. Vatolin, Y.S. Kozlov, and E.A. Pastukhov: *Russ Met.*, 1977, vol. 5, pp. 181–83.
34. I. Arpshofen, M.J. Pool, U. Gerling, F. Sommer, U. Gerling, E. Predel, and B. Schultheiss: *Z. Metallkde.*, 1981, vol. 72, pp. 776–81.
35. R. Castanet, R. Chastel, and C. Bergman: *J. Chem. Thermodyn.*, 1983, vol. 15, pp. 773–77.
36. L. Topor and O.J. Kleppa: *Z. Metallkd*, 1986, vol. 77, pp. 65–71.
37. R. Castanet and R. Chastel: *Z. Metallkde.*, 1987, vol. 78, pp. 97–102.
38. T. Kang and R. Castanet: *J. Less Common Metals*, 1977, vol. 51, pp. 125–35.
39. C. Bergman, N. Kayama, M. Gilbert, R. Castanet, and J.C. Mathieu: *J. Phys. Coll.*, 1980, vol. C8, pp. 591–94.
40. M.S. Chandrasekharaiah: *J. Alloy Phase Diagr.*, 1989, vol. 14, pp. 105–16.
41. B. Aronsson and A. Nylund: *Acta Chem. Scand.*, 1960, vol. 14, pp. 1011–18.
42. W. Wopersnow and K. Schubert: *Z. Metallkde.*, 1976, vol. 67, pp. 807–10.

Author Proof
UNCORRECTED PROOF

Journal : MMTA Dispatch : 28-10-2015 Pages : 15
PIPS No. : 3206 ☐ LE ☐ TYPESET
MS Code : ☐ CP ☐ DISK